ADVANCED FUNCTIONAL MATERIALS
www.afm-journal.de

Synthetic Surfaces with Robust and Tunable Underwater Superoleophobicity

*Uttam Manna and David M. Lynn**

Surfaces with extreme wetting properties are useful for the collection, manipulation, transport, and avoidance of aqueous and organic fluids of commercial and strategic importance. Two major obstacles to the deployment of synthetic non-wetting materials in practical scenarios are their lack of mechanical durability and their susceptibility to fouling in contaminated or chemically complex media. Here, crosslinked and nanoporous polymer multilayers are reported that overcome these limitations and exhibit robust and tunable "underwater superoleophobicity", or the ability to almost completely prevent contact with oils and other organic fluids when submerged in water. These entirely organic coatings mimic key chemical and structural features found on the scales of fish and other natural anti-oil-fouling surfaces, and are remarkably tolerant to physical, chemical, and environmental insults commonly encountered in natural and synthetic aqueous environments. This approach also permits facile manipulation and patterning of surface chemistry and, thus, tunable spatial control over other important aspects of interfacial behavior, such as underwater oil adhesiveness, that extend and expand the potential utility of synthetic anti-oil-fouling surfaces in aqueous, aquatic, and marine environments.

1. Introduction

Surfaces with extreme wetting properties are of special interest and practical utility in many commercial, industrial, military, and biotechnological contexts. Synthetic materials that are completely non-wetting to water (superhydrophobic),[1,2] oils (superoleophobic),[3,4] or both oil and water (superomniphobic)[5,6] have enabled the design of self-cleaning and anti-fouling surfaces, new generations of smart textiles and stain-resistant clothing, and innovative methods for the collection and manipulation of complex fluids, including approaches to oil recovery and oil/water separation.[7–15] Advances toward these and other emerging applications have been made possible by (i) an understanding of the ways that features found on natural non-wetting surfaces (e.g., the lotus leaf)[16] work in synergy to promote anti-fouling behavior,[17] and (ii) by the development of new approaches to the fabrication of hard and soft material interfaces[18] that can recapitulate those critical features on synthetic surfaces better suited for everyday use (so-called "bio-inspired" approaches to materials design).

One major challenge to the application of synthetic non-wetting surfaces in practical settings lies in developing materials that are durable and able to withstand the rigors of use without loss of special wetting behavior.[5,19–21] The susceptibility of many synthetic non-wetting surfaces to physical insults, for example, is commonly regarded as an "Achilles heel" with respect to practical utility.[22,23] Other key challenges lie in developing anti-fouling interfaces that remain functional in harsh and chemically complex media—e.g., at extremes of pH and ionic strength, or upon contact with surface-active agents that can also adsorb and compromise non-wetting behavior.[8] Non-wetting surfaces that permit interfacial properties to be tuned or spatially patterned could also open the door to new and advanced applications of these "super-phobic" materials.[13,24]

The work reported here was motivated by recent reports of materials that exhibit "underwater superoleophobicity",[15,25–29] or surfaces that are extremely non-wetting to oils and organic liquids only when submerged in water. This unique behavior contrasts to that of conventional superoleophobic materials, on which organic liquids "bead up" and "roll off" when brought into contact under air[3] (superoleophobicity is defined here by an advancing oil contact angle (θ) ≥ 150° and a roll-off angle ≤10°). Surfaces that exhibit superoleophobicity only when wet provide new principles for the design of anti-fouling surfaces and the collection, transport, or separation of oils and other organic fluids in underwater environments, including industrially and strategically important aquatic and marine environments.

Synthetic surfaces that exhibit underwater superoleophobicity have emerged only recently, based on designs that mimic, to varying extents, critical physical and chemical features found on the scales of fish[25,29] and other aquatic anti-oil-fouling surfaces.[27,28] These materials typically have two key elements in common: (i) rough surfaces that present micro- and nanoscale topographic features, and (ii) an ability to adsorb or host water near their surfaces to minimize contact

Dr. U. Manna, Prof. D. M. Lynn
Department of Chemical & Biological Engineering
University of Wisconsin–Madison
1415 Engineering Drive, Madison, WI 53706, USA
E-mail: dlynn@engr.wisc.edu
Prof. D. M. Lynn
Department of Chemistry
University of Wisconsin–Madison
1101 University Avenue, Madison, WI 53706, USA

DOI: 10.1002/adfm.201403735

with oily liquids[15,25] (creating a conceptual and theoretical framework similar in principle to superhydrophobic surfaces with multiscale features that can "trap" air to repel water). Previous studies have used hydrogels,[25,30] polyelectrolyte assemblies,[31–33] and metal oxide nanorods[34,35] to create model surfaces meeting these criteria. Those approaches have advanced an understanding of key principles underlying underwater superoleophobicity, but they lead to soft surfaces and coatings that are susceptible to physical damage or disruption, particularly in harsh and chemically complex environments. They also provide limited means to tune non-wetting behavior or define and vary other important physicochemical or interfacial properties.

Here we report thin polymer coatings that exhibit robust underwater superoleophobicity and remarkable structural and functional tolerance to a broad range of physical, chemical, and environmental challenges encountered by surfaces deployed in aqueous or aquatic environments. These entirely organic anti-fouling coatings can be applied to surfaces of arbitrary shape, size, and composition and provide straightforward means to manipulate surface chemistry and, thereby, fine-tune other useful features of their interfacial behavior. Our results address important obstacles to the deployment of synthetic "superphobic" materials in applied settings, provide guiding principles for the design of new classes of durable anti-fouling and oil-resistant surfaces, and establish a framework for the investigation of molecular-level and nanoscale design features that expand the range of properties of synthetic surfaces that exhibit extreme anti-oil-fouling behaviors.

2. Results

2.1. Fabrication and Characterization

Our approach is based on the covalent layer-by-layer assembly of polymer multilayers using branched poly(ethyleneimine) (PEI) and the amine-reactive polymer poly(vinyl-4,4-dimethylazlactone) (PVDMA).[36] This general approach yields coatings that are chemically crosslinked (owing to the formation of chemically stable amide/amide linkages during assembly)[36] and contain amine-reactive azlactone groups that can be used to define and tailor interfacial properties after assembly (by treatment with molecules containing primary amines).[37–40] We performed a series of initial experiments to compare the interfacial properties of PEI/PVDMA multilayers brought into contact with aqueous and organic fluids in air and when submerged underwater. For these studies, we fabricated multilayers from 10 layer-pairs of PEI and PVDMA using a procedure that leads to thin and porous films with enhanced surface roughness (vide infra); these films were then functionalized by reaction with the model carbohydrate D-glucamine to install hydrophilic hydroxyl groups.[37]

These coatings were 1.1 ± 0.4 μm thick and were readily and rapidly wet by droplets of water (colored green; **Figure 1**a) and the model oil dichloroethane (DCE, colored red; ρ = 1.25 g mL^{-1}; Figure 1b) under air ($\theta \approx 0°$). In contrast, these coatings were extremely non-wetting to DCE when they were submerged in water (Figure 1c). Small droplets of DCE (10 μL) settled onto submerged surfaces with contact angles of ≈161° (Figure 1d), and rolled off immediately if surfaces were not held

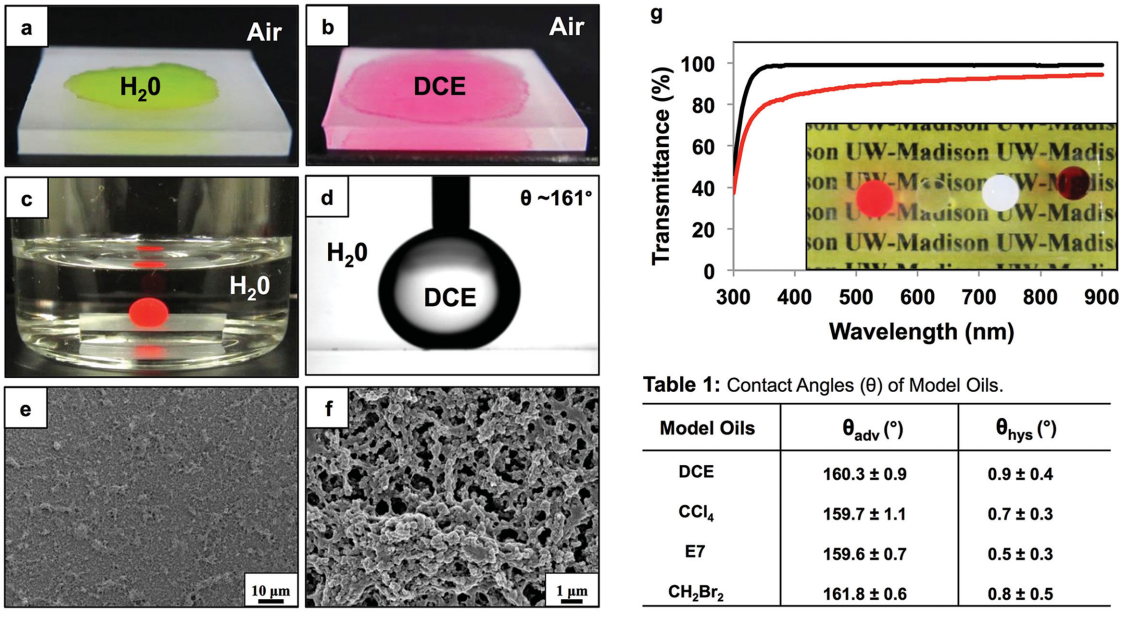

Table 1: Contact Angles (θ) of Model Oils.

Model Oils	θ_{adv} (°)	θ_{hys} (°)
DCE	160.3 ± 0.9	0.9 ± 0.4
CCl_4	159.7 ± 1.1	0.7 ± 0.3
E7	159.6 ± 0.7	0.5 ± 0.3
CH_2Br_2	161.8 ± 0.6	0.8 ± 0.5

Figure 1. Physical and interfacial characterization of underwater superoleophobic polymer multilayers. a,b) Digital images of planar glass substrates coated with glucamine-functionalized multilayers showing wetting of water (green; a)) and dichloroethane (DCE, red; b)) on dry films under air. c,d) Images showing beading of c) a droplet of DCE (red) and d) the advancing underwater oil contact angle ($\theta \approx 161°$) when the coatings are submerged in water. e,f) Low and high magnification SEM images of porous multilayers. g) Percent transmittance versus λ for bare glass (black) and coatings fabricated on glass substrates (red) when submerged underwater; inset shows optical transparency and the beading of four model oils (DCE, CCl_4, the liquid crystal (E7), and CH_2Br_2; dyes added to DCE and CH_2Br_2 to enhance visual contrast). Table 1 shows underwater advancing contact angles and associated hysteresis for these four oils. Data represent mean ± s.d. (n = 5).

perfectly level (with a contact angle hysteresis, or "roll-off" angle, of ≈1°; Figure S1, Supporting Information). Droplets of DCE dropped under water from a distance of 5 cm bounced freely on these surfaces (Figure S2, Supporting Information), further revealing low oil adhesiveness. These coatings were also superoleophobic to other model oils, including CCl_4, CH_2Br_2, and the thermotropic liquid crystal E7 ($\theta \approx 160°$–$162°$, see Figure 1g, inset and Table 1; oils used here were selected to be more dense than water (ρ = 1.59 g mL^{-1}, 2.47 g mL^{-1}, and 1.03 g mL^{-1}, respectively) to facilitate characterization of θ). As revealed in Figure 1g, these coatings were optically transparent when wet, with a transmittance ≈90% that of glass at $\lambda > 500$ nm. This feature broadens the range of applications for which these materials are suited, and permits use of optical methods to interrogate and characterize the behaviors of non-wetting liquids (e.g., μ-scale droplets of oil-in-water emulsions, etc.)

Characterization of these coatings by scanning electron microscopy (SEM) revealed substantial nanoscale porosity and the presence of both micro and nanoscale topographic features (Figure 1e,f). The underwater superoleophobicity of these thin films depended critically upon the presence of these features; otherwise identical smooth films devoid of these features did not exhibit underwater superoleophobicity ($\theta \approx 142°$, with high hysteresis (≈19°); see Figure S3, Supporting Information). The origins of these features are not completely understood, but they appear to result, at least in part, from the reactive deposition of nanoscale aggregates of PEI and PVDMA during assembly; protocols that prevented the formation of these aggregates lead to smooth films that lacked these features (Figure S3, Supporting Information). The methods used here to coat planar glass surfaces could also be used to rapidly and reproducibly deposit uniform and porous superoleophobic coatings on other objects of diverse shape, size, and composition (vide infra).

2.2. Tolerance to Physical, Chemical, and Environmental Challenges

The crosslinked and porous features of these coatings combine to endow them with remarkable tolerance to a wide range of different physical, chemical, and environmental challenges that can compromise non-wetting interfaces and are well-known to damage or disrupt hydrogels and polyelectrolyte assemblies used to design other synthetic underwater oil-repellant surfaces. We first characterized the morphologies and wetting behaviors of our coatings using two tests used to characterize the durability of conventional non-wetting surfaces.[5,20] In the first test, sand grains were dropped onto dry coatings from a height of 20 cm (**Figure 2**a,b; setup shown in Figure S4, Supporting Information). In the second test, adhesive tape was applied with a pressure of ≈445 kPa and then peeled off (Figure 2c,d). No large-scale erosion, cracking, or peeling was observed, in either case, by visual inspection. Further characterization by SEM revealed no changes in micro/nanoscale morphology in response to these insults (Figure 2b,d), and the underwater oil contact angles of both films remained unchanged ($\theta \approx 159°$ and hysteresis of ≈1°; Figure 2a,c and Table 2).

Repeated abrasion with sandpaper resulted in scratching and the removal of substantial amounts of material from these coatings (Figure 2i). Remarkably, however, this severe physical damage did not impact underwater superoleophobicity ($\theta \approx 161°$, hysteresis of ≈1°; Figure 2j,o,p and Table 2). SEM characterization of these severely scratched coatings revealed abrasion of these porous multilayers to expose new microscale and nanoscale topography with physical and chemical features sufficient to maintain extreme anti-oil-fouling behavior (Figure 2k–n). Thus, while these crosslinked surfaces are not able to completely resist all forms of physical damage, their porous structures provide them with means to tolerate severe insults without loss of underwater non-wetting behavior. This property is unique and similar to that of several recently reported porous superhydrophobic materials,[5,21,41] and it substantially increases the durability and potential utility of these surfaces relative to other synthetic underwater anti-oil-fouling coatings.

To characterize physical stability when hydrated, we performed two other tests in which (i) 50 g of solid glass beads (diameter = 2–3 mm) were dropped onto coatings submerged under 15 cm of water (setup shown in Figure S4, Supporting Information), and (ii) films were exposed to water ejected from a rapidly flowing faucet for 30 min (flow rate = 100 mL s^{-1}; nozzle velocity = 127.4 cm s^{-1}; distance of the surface from nozzle ≈2 cm; see the Experimental Section for additional details). These challenges had no apparent impact on film morphology (Figure 2f) or wetting behavior ($\theta \approx 159°$–$160°$, hysteresis of ≈1°; Figure 2e and Table 2). Finally, coatings fabricated on sheets of poly(ethylene terephthalate) (PET) permitted characterization of the influence of flexing and bending on physical and functional integrity. Coatings fabricated on PET exhibited micro/nanoscale morphologies and wetting behaviors similar to those deposited on glass ($\theta \approx 161°$; Figure S5, Supporting Information) and remained anti-fouling after repeated bending and permanent creasing (e.g., Figure 2g,h, Table 2, and Figure S5, Supporting Information; $\theta \approx 161°$ after creasing).

Coatings boiled in water for 1 h or exposed to autoclave steam cycles did not delaminate and remained non-wetting after cooling to ambient temperature ($\theta \approx 160°$, hysteresis of ≈1°; Table 2). Coatings frozen into blocks of ice also retained their anti-fouling properties; freeze/thaw cycles were repeated at least 10× without loss of underwater superoleophobicity ($\theta \approx 160°$, with hysteresis of ≈1° after 10 cycles; Table 2). We conclude that these coatings can withstand the extremes of temperature and full range of associated water phase changes likely to be encountered during use in synthetic or natural aqueous environments. The ability to withstand autoclaving provides opportunities to exploit these anti-fouling surfaces in contexts where sterilization is critical.

We also investigated the impact of harsh chemical environments and media of increasing complexity on film integrity and non-wetting behavior, including exposure to (i) extremes of pH and ionic strength and (ii) surface-active agents and other species (surfactants, lipids, and proteins) known to adsorb at interfaces and cause changes in wettability. Coatings submerged in solutions of HCl (0.5 M, pH = 1) and NaOH (0.5 M, pH = 11) for 30 min remained superoleophobic (Table 2; $\theta \approx 160°$) with low oil adhesion (hysteresis ≈1°). Films incubated in high concentrations of cationic, anionic, and nonionic surfactants [5.0 M sodium dodecyl sulfate (SDS) or dodecyltrimethylammonium bromide (DTAB), and Triton X-100 (1.0 M)] and mammalian cell

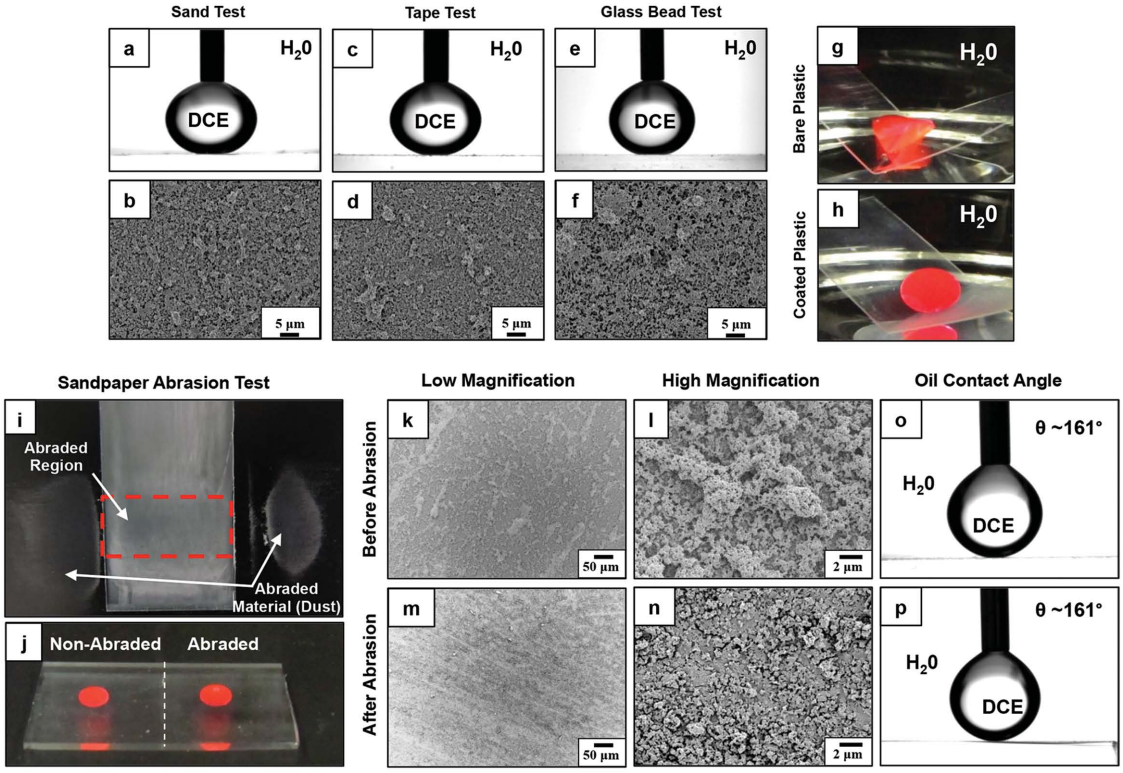

Table 2: Results of Physical and Chemical Tests.

Tests	θ_{adv} (°)	θ_{hys} (°)
Sand Test	159.2 ± 1.1	0.9 ± 0.6
Sandpaper Test	161.2 ± 0.9	0.9 ± 0.7
Tape Test	159.4 ± 0.8	1.0 ± 0.5
Glass Bead Test	158.9 ± 1.2	0.9 ± 0.4
Water Stream	160.6 ± 0.9	0.9 ± 0.5
Boiling Water	159.7 ± 0.8	0.8 ± 0.7
Autoclaving	160.2 ± 0.7	0.9 ± 0.6
Freezing Water	159.9 ± 0.9	1.0 ± 0.8
Acidic Water (pH 1)	159.8 ± 1.1	0.9 ± 0.8
Alkaline Water (pH 11)	160.2 ± 0.9	1.1 ± 0.7
Bending & Creasing	161.1 ± 0.8	0.9 ± 0.7

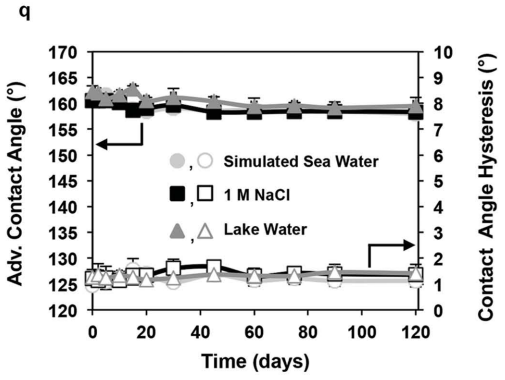

Figure 2. Physical, chemical, and environmental stability of underwater superoleophobic multilayers. a,c,e) Advancing underwater oil contact angles and b,d,f) SEM images of glucamine-functionalized underwater superoleophobic coatings after exposure to a,b) falling sand ($\theta \approx 159°$), c,d) peeling of adhesive tape ($\theta \approx 161°$), and e,f) glass beads dropped under water ($\theta \approx 159°$). g,h) Wetting of droplets of DCE (red) on thin sheets of bare PET g) or PET coated with a glucamine-functionalized coating h); samples were bent and creased prior to placement of the droplets (see text). i) Results of sandpaper abrasion tests, showing a digital picture of a film-coated glass slide abraded by repeated manual rubbing (25 times) with sandpaper (red box; abraded material removed from the surface of the coating as a result of this treatment is shown at the sides of the image). j) Two droplets of DCE placed on the surface of a submerged glucamine-functionalized multilayer coating that was abraded with sandpaper (right: abraded region; left: non-abraded region). k–n) Low- and high-magnification SEM images of coatings before and after abrasion, and o,p) underwater oil contact angle measurements on o) non-abraded ($\theta \approx 161°$) and p) abraded coatings ($\theta \approx 161°$). Table 2 shows underwater advancing contact angles and associated hysteresis for coatings exposed to physical, chemical, and environmental challenges. Data represent mean ± s.d. ($n = 5$). q) Plot showing contact angles and hysteresis for coatings exposed to simulated seawater, 1.0 M NaCl, and lake water for four months. Data represent mean ± s.d. ($n = 5$).

culture media containing 10% serum did not exhibit changes in non-wetting behavior for at least 45 days (Figure S6, Supporting Information). We also assessed the potential utility of these coatings in marine environments and other high ionic strength media by incubating them in simulated seawater and solutions of 1.0 M NaCl (Figure 2q); the advancing oil contact angles of these surfaces remained above 158° (with hysteresis < 2°) for at least 4 months under these conditions. Finally, to assess stability in other complex aquatic environments, coatings were submerged in eutrophic lake water containing

well-characterized concentrations of dissolved and suspended organic matter, inorganic compounds, and microbial flora.[42,43] Underwater superoleophobicity remained unaffected by the components of this complex medium for at least 4 months (Figure 2q).

2.3. Chemical Manipulation and Spatial Patterning of Underwater Oil Adhesiveness

The reactive process used to assemble these crosslinked multilayers leaves behind residual azlactone groups that enable installation of secondary surface functionality (e.g., glucamine, vide supra).[36] This unique feature allowed us to systematically vary and characterize the impact of different chemical motifs on non-wetting properties while maintaining all other nano- and microscale topographic features constant (**Figure 3**a). Surfaces treated to present positively or negatively charged groups (quaternary amines (2) or carboxylates (3); Figure 3a) remained hydrophilic and exhibited underwater oil contact angles of ≈158° (hysteresis ≈1°). Combined with the results above for hydroxyl-functionalized films (1), these results reveal surface hydrophilicity itself, and not the specific chemical nature of the groups that confer it, to be the principal chemical factor impacting maintenance of superoleophobicity.

Interestingly, when these films were functionalized with hydrophobic propyl (C_3) groups (4), advancing underwater contact angles did not change significantly ($\theta \approx 158°$; Table 3 and Figure 3d). However, the contact angle hysteresis for these hydrophobically modified films increased substantially (from ≈1° to ≈23°; Table 3 and Figure 3d,e), revealing an increase in oil adhesiveness (hysteresis provides a quantitative measure of oil adhesiveness; deformation of the receding droplet shown in Figure 3e and additional results shown in Figure S7, Supporting Information, provide visual indications). Decoration with more hydrophobic octyl (C_8) groups (5) also did not influence θ significantly (≈158°), but hysteresis increased substantially to ≈42° (Table 3 and Figure 3f,g). Longer decyl (C_{10}) groups (6) resulted in a reduction of the advancing contact angle (to ≈146°), but no further increase in droplet roll-off angles (hysteresis remained at ≈44°; Table 3 and Figure 3h,i). These changes in wetting behavior and adhesiveness arise solely from differences in the chemical structures (and thus the relative surface energies) of these hydrophobically modified films; characterization by SEM revealed no change in nano/microscale topography after chemical functionalization (Figure S7, Supporting Information). Taken together, these results provide the basis of a chemical and molecular-level approach that can be used to tune underwater oil adhesiveness—i.e., to create synthetic surfaces that are either (i) non-wetting and non-adhesive to oils (using

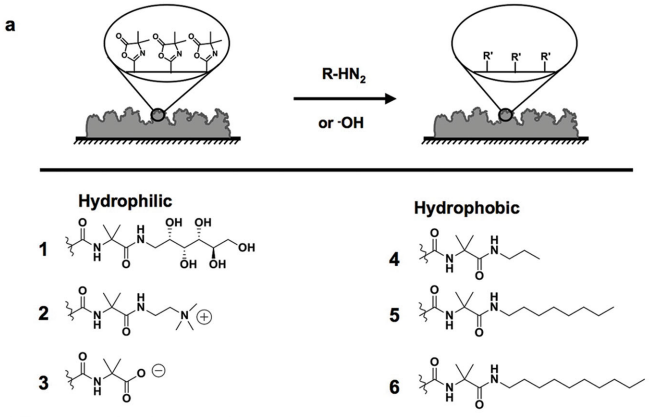

Table 3: Contact Angles of Chemically-Functionalized Films.

	Film Functionality	θ_{H2O} in air (°)	θ_{DCE} in air (°)	θ_{DCE} under H_2O (°)	θ_{hys} (°)
Hydrophilic	-Gluc (1)	~0	~0	160.3 ± 0.9	0.9 ± 0.4
Hydrophilic	-NR_3^+ (2)	~0	~0	158.9 ± 1.6	0.7 ± 0.3
Hydrophilic	-COO^- (3)	~0	~0	158.1 ± 1.1	0.9 ± 0.3
Hydrophobic	-Propyl(4)	67.3 ± 3.9	~0	157.8 ± 0.8	23.1 ± 2.1
Hydrophobic	-Octyl(5)	108.4 ± 4.5	~0	158.1 ± 1.6	42.4 ± 3.2
Hydrophobic	-Decyl(6)	116.5 ± 3.2	~0	145.6 ± 2.1	44.2 ± 4.4

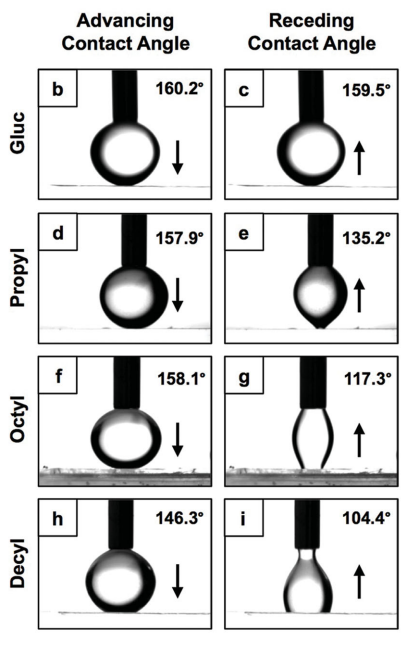

Figure 3. Chemical functionalization and tuning of the underwater oil adhesiveness of underwater superoleophobic multilayers. a) Schematic illustration of azlactone-functionalized multilayers (top left) and the reactive process used to install secondary chemical functionality. Also shown are the chemical structures of the hydrophilic (1, 2, 3) and hydrophobic (4, 5, 6) functionality investigated in this study. Table 3 shows (i) the advancing contact angles of water and DCE under air and (ii) the advancing underwater oil contact angle and hysteresis for these chemically functionalized films. Data represent the mean ± s.d. ($n = 5$). b,d,f,h) Underwater advancing contact angles and c,e,g,i) underwater receding contact angles of droplets of DCE on coatings functionalized with glucamine [b) $\theta \approx 160°$; c) $\theta \approx 159°$], propylamine [d) $\theta \approx 158°$; e) $\theta \approx 135°$], octylamine [f) $\theta \approx 158°$; g) $\theta \approx 117°$], and decylamine [h) $\theta \approx 146°$; i) $\theta \approx 104°$].

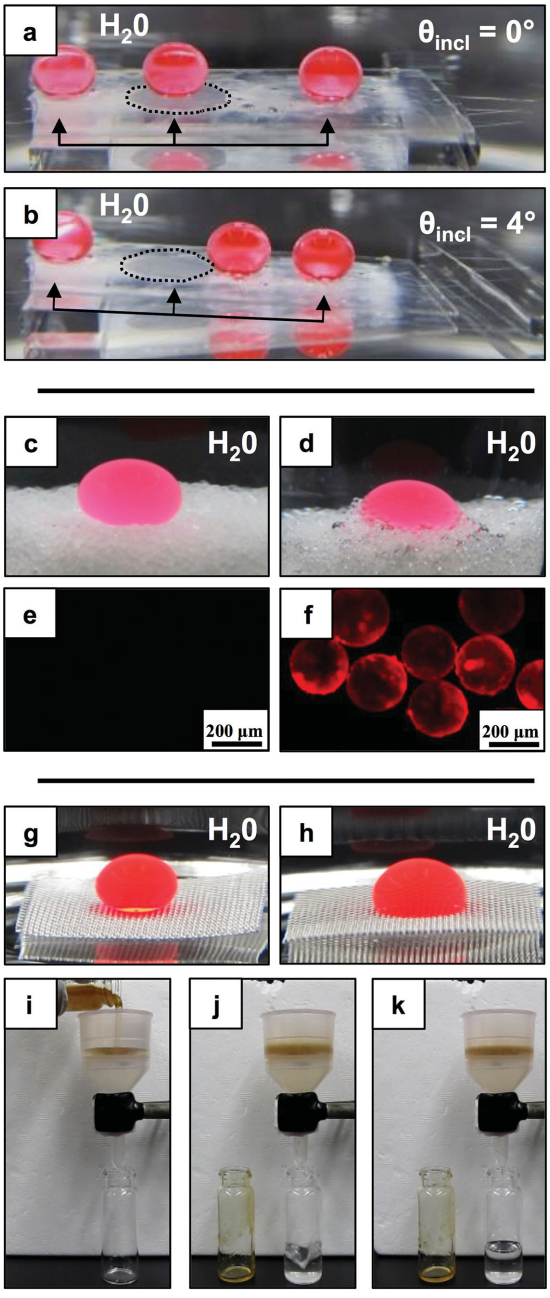

Figure 4. Chemical patterning and fabrication of underwater superoleophobic multilayers on topologically complex substrates. a,b) Images showing behavior of droplets of DCE (red) on the surface of a submerged glass slide patterned with a small (≈3 mm diameter) circular region functionalized to be superoleophobic and non-adhesive (dotted circle); the remainder of the surface was functionalized to be superoleophobic but adhesive (by treatment with propylamine; see text). Droplets placed in adhesive regions (left and right) remained in place when the substrate was tilted at an angle (θ_{incl}; e.g., 4° is shown) lower than that of the contact angle hysteresis. a) Droplets placed in the non-adhesive region (center) rolled downhill but b) became pinned upon rolling into contact with the adhesive region (center-right). c,d) Droplets of DCE (red, 15 μL) placed on a bed of glass beads coated with c) glucamine-functionalized multilayers or d) bare glass beads. e) Fluorescence microscopy images reveal no adsorption of DCE (stained red) on beads coated with glucamine-functionalized films after incubation with DCE/water emulsions (see text and Figure S8, Supporting Information). The presence of bright red signal in (f) indicates adsorption of DCE to control beads coated with adhesive decylamine-functionalized films. g) Beading of a droplet of DCE on stainless steel mesh coated with glucamine-functionalized multilayers. h) Wetting of a droplet of DCE on a sample of bare (uncoated) mesh. i–k) Images demonstrating gravity-driven separation of motor oil and water promoted by pouring oil/water mixtures through mesh coated with glucamine-functionalized multilayers. j) Water passes through rapidly into a collection vessel; k) oil remains suspended on top of the mesh and can be recovered in near quantitative yields.

hydrophilic groups) or (ii) superoleophobic, but with tunable degrees of oil adhesiveness (by varying the structures of lower-energy hydrophobic groups).

These two conditions are similar in some respects to the non-adhesive Cassie–Baxter[44] and adhesive Wenzel[45] states used to describe the behavior of water on superhydrophobic surfaces. Our results thus suggest principles that can be used to capture, release, pattern, and manipulate the transport of organic fluids on surfaces in aquatic environments. As proof of concept, **Figure 4**a shows a submerged glass slide coated with a superoleophobic but adhesive (propyl-functionalized) film and a small, circular region spatially patterned to be non-wetting and non-adhesive (dotted circle; see the Experimental Section). Droplets of DCE placed in both regions remained stationary when the substrate was held perfectly horizontal (Figure 4a). Droplets placed in adhesive areas remained pinned and did not roll off when the substrate was tipped slightly (e.g., θ_{incl} = 4°). The droplet in the non-adhesive patterned region rolled downhill, but became pinned upon contact with the adhesive region of the pattern (Figure 4b). These arrested droplets could be dislodged and induced to roll again by tipping substrates at angles >23° or by inducing flows in the surrounding liquid.

2.4. Complex Substrates and Surfaces

The process used to assemble these coatings also enables fabrication of underwater superoleophobic surfaces on a wide range of macroscale and microscale objects, including curved surfaces. Two examples of potential utility are described here to demonstrate proof of principle. Figure 4c shows a pile of glass microspheres (diameter = 200–300 μm) coated with glucamine-functionalized films. Characterization of these beads by SEM revealed topographic features similar to those found on planar surfaces (Figure S8, Supporting Information), and bead-beds created from these coated microspheres were non-wetting to DCE in underwater environments ($\theta \approx 163°$, hysteresis ≈1°; Figure 4c, a droplet of DCE on a pile of bare glass beads is shown in Figure 4d). It was not possible to characterize the oleophobicity of individual beads by measurement of contact angles. However, experiments using beads dispersed in water/DCE emulsions revealed individual beads to be strongly oleophobic (Figure 4e; relative to glass beads coated with adhesive decyl-functionalized films, Figure 4f).

Finally, Figure 4g shows stainless steel wire mesh (pore size ≈126 μm) coated with glucamine-functionalized films (see also Figure S9, Supporting Information). These coatings prevented wetting by oils ($\theta \approx 162°$ with a hysteresis of ≈1° for

DCE), and could be flexed and bent into useful shapes without loss of underwater superoleophobicity. The superhydrophilic but superoleophobic nature of these coated meshes prevented transport of oils through the pores of the mesh, but permitted the passage of water, providing a basis for gravity-driven separation of oil/water mixtures.[12,35] Figure 4i–k demonstrates proof of principle using a device constructed from coated mesh and a two-piece plastic funnel. This simple setup permitted low-energy separation of mixtures of water and motor oil (5:1, v/v; $\rho = 0.843$ g mL^{-1}); water passed rapidly through the mesh into a collection container (Figure 4j), and oil free of bulk water accumulated on the mesh (Figure 4k) and was recovered in near-quantitative yields (Figure S10, Supporting Information). This process could be repeated multiple times and degrees of separation were unaffected when more complex oil/water mixtures prepared with acidic water (pH = 1), alkaline water (pH = 11), simulated seawater, and lake water were used (Figure S10, Supporting Information).

3. Discussion

The synthetic coatings reported here mimic key chemical and structural features found on natural underwater oil-repellent materials.[25,27–29] Our results demonstrate these entirely organic materials to be mechanically durable, functionally tolerant to severe physical abrasion, and to retain their anti-fouling properties upon prolonged exposure to chemically complex media—outcomes that we attribute to the crosslinked nature of the films, the chemical stability of their amide/amide-based crosslinks, and their porous structures. These unique features, along with the substrate independence of the methods used for assembly, substantially increase the potential utility of these materials in different aqueous, aquatic, and marine environments relative to synthetic oil-repellant surfaces assembled using weak interactions or constructed from soft, brittle, or chemically erodible materials.[25,31,32,35]

The dependence of non-wetting behavior on surface topography and hydrophilicity is consistent with previous investigations of the structures and behaviors of underwater oil-repellant surfaces. Relative to past approaches to the design of synthetic underwater superoleophobic surfaces, however, our approach yields amine-reactive coatings that allow surface chemistry to be varied systematically and orthogonally to all other surface and microstructural features. This feature is significant in several ways. First, reactivity provides means to probe and dissect the influence of surface chemistry on non-wetting behavior in ways that are independent of surface topography. Our results confirm surface hydrophilicity to be critical to the maintenance of superophobicity, but also reveal this property to be tolerant to the variation of exposed hydrophilic groups over a broad range of structural and functional space (e.g., from neutral hydroxyl functionality to formally charged cationic or anionic groups). We note here that prior studies demonstrate surfaces decorated with D-glucamine, including self-assembled monolayers (SAMs) on gold[46,47] and nonporous PEI/PVDMA multilayers deposited on glass,[37] to resist fouling by proteins and cells. We did not quantify the ability of our porous and superoleophobic surfaces to prevent adsorption of surfactants or proteins here, but our results reveal that prolonged exposure to proteins and other surface-active agents does not compromise anti-oil-fouling behavior. When combined, these and other unique features of this system provide a platform for the design of multifunctional interfaces that could prevent fouling by organic fluids and other substances, organisms, or environmental contaminants (or perform other useful secondary functions) more effectively.

Second, our results establish the basis of an approach that can be used to vary and systematically tune the oil adhesiveness of underwater superoleophobic surfaces. The ability to create surfaces with spatially defined regions that contrast sharply in oil adhesiveness provides new principles for the capture and manipulation of organic fluids in aqueous media. In combination with more sophisticated methods for the deposition and spatial patterning of amine-based "inks," this approach could be used to create macroscale or microscale patterns or devices that enable passive or active control over the wetting behaviors of oils (e.g., to pattern bulk fluids or facilitate and direct the reversible capture and transport of emulsion droplets in microfluidic contexts, etc.). This degree of control over the patterning of adhesive and non-adhesive surface features is difficult to achieve using other methods for the design of underwater superoleophobic surfaces.[48]

Finally, we note that while the crosslinked and porous nature of these coatings is a strength with respect to durability and stability in harsh media, the coating/substrate interface itself presents a potential weak link. We did not observe significant delamination of coatings under conditions investigated here, including in experiments for which substrates were boiled, frozen/thawed, or incubated at extremes of pH or ionic strength. We mention, however, that the amine-reactive azlactone groups of PVDMA also provide means to covalently attach these coatings to substrates bearing amine functionality,[49] including protein-based structures with exposed lysine groups.[38] Judicious selection or optimization of substrate design could thus provide other routes to improving performance that are not accessible with coatings assembled using other methods.

The soft material interfaces reported here address key obstacles to the application of non-wetting surfaces and anti-fouling "super-phobic" materials in practical, real-world scenarios. We anticipate that the principles and properties reported here will be useful for the design of durable and injury-tolerant oil-repellant coatings and the development of advanced, multifunctional surfaces that enable new means of control over the capture, transport, manipulation, and separation of oils and other organic fluids in fundamental and applied contexts.

4. Experimental Section

Materials: 2-Vinyl-4,4-dimethylazlactone (VDMA) was a gift from Dr. Steven M. Heilmann (3M Corporation, Minneapolis, MN). Poly(2-vinyl-4,4-dimethylazlactone) (PVDMA) was synthesized by free-radical polymerization of VDMA both in the presence (MW ≈20 700, PDI 2.4) and absence (MW ≈3 700, PDI 2.4) of 7 wt% of intentionally added cyclic azlactone-functionalized oligomer, as described previously.[50] Branched poly(ethylene imine) (PEI; MW ≈25 000), *n*-propylamine, *n*-octylamine, *n*-decylamine (95%), acetone (HPLC grade), tetrahydrofuran (THF, HPLC grade), dichloroethane (DCE), carbon tetrachloride (CCl_4),

dibromomethane (CH_2Br_2), magnesium sulfate, calcium chloride, hydrochloric acid (HCl), sodium hydroxide (NaOH), sodium dodecyl sulfate (SDS), dodecyltrimethylammonium bromide (DTAB), and Nile red were purchased from Sigma-Aldrich (Milwaukee, WI). D-Glucamine (>95%) was purchased from TCI America (Portland, OR). Triton X-100 was obtained from Promega (Madison, WI). Dimethylaminopropylamine (DMAPA) and iodine were purchased from Acros (New Jersey, USA). The thermotropic liquid crystal E7 was purchased from Licristal (Japan). Sodium chloride (NaCl), magnesium chloride ($MgCl_2$), glass microscope slides, and solid glass beads having a diameter of 200–300 μm were purchased from Fisher Scientific (Pittsburgh, PA). Dulbecco's modified Eagle's medium (DMEM), Opti-MEM cell culture medium, and fetal bovine serum (FBS) were purchased from Invitrogen (Carlsbad, CA). Valvoline motor oil was obtained from CITGO Petroleum Corporation (Oklahoma). Thin sheets of poly(ethylene terephthalate) (PET) film (0.004 in. thick) were purchased from McMaster Carr. Stainless steel wire mesh was obtained from MSC Industrial Supply Co. (Melville, NY). Adhesive tape was purchased from 3M Corporation. Deionized water with a resistance of 18.2 MΩ was used to prepare aqueous phases used in all experiments unless otherwise noted. Samples of eutrophic lake water were collected from Lake Mendota (Madison, WI). All chemicals were used as received without further purification unless otherwise noted.

General Considerations: Scanning electron micrographs were acquired using a LEO DSM 1530 scanning electron microscope at an accelerating voltage of 3 kV. Prior to imaging, samples were coated with a thin layer of gold using a gold sputterer operating at 45 mA under a vacuum pressure of 50 mTorr for 40 s. Digital pictures were acquired using a Canon PowerShot SX130 IS digital camera. Advancing and receding contact angle measurements were made using a Dataphysics OCA 15 Plus contact angle goniometer at ambient temperature using 10 μL of model oils both in air and under water; a minimum of five measurements was made in at least five locations on each film. The optical thicknesses of films were characterized using a Gaertner LSE ellipsometer (632.8 nm, incident angle = 70°). Data were processed using the Gaertner Ellipsometer Measurement Program. Relative thicknesses were calculated assuming an average refractive index of 1.577 for the polymer multilayers. Thicknesses were determined in at least five different standardized locations on each substrate and are presented as an average with standard deviation. Characterization of optical transparency was performed using a Beckman Coulter DU520 UV–vis Spectrophotometer (Fullerton, CA). Simulated seawater was prepared by dissolving NaCl (26.73 g), $MgCl_2$ (2.26 g), $MgSO_4$ (3.25 g), and $CaCl_2$ (1.12 g) in 1.0 L of water. Compressed air used to dry samples was filtered through a 0.2 μm membrane syringe filter.

Fabrication of Reactive Polymer Multilayers: Porous polymer multilayers exhibiting microscale and nanoscale topographic features were fabricated on planar glass substrates using the following general procedure: (i) substrates were submerged in a solution of PEI (20×10^{-3} M in acetone with respect to the polymer repeat unit) for 20 s; (ii) substrates were removed and immersed in an initial acetone bath for 20 s, followed by a second acetone bath for 20 s; (iii) substrates were submerged in a solution of PVDMA (20×10^{-3} M in acetone with respect to the polymer repeat unit) for 20 s; and (iv) substrates were removed and rinsed again using the procedure outlined under step (ii). This cycle was repeated 10 times to fabricate multilayers consisting of 10 PEI/PVDMA layer pairs. For these experiments, the concentrations of polymer solutions were maintained constant by addition of acetone as needed to compensate for solvent evaporation, and rinse baths were not replaced with fresh acetone during film fabrication. For the fabrication of these thicker (≈1.1 μm thick) and rougher films, PVDMA synthesized in the presence of 7 wt% of intentionally added cyclic azlactone-functionalized oligomer was used (see above). Procedures used to fabricate thinner (≈60 nm thick) control coatings that did not exhibit significant porosity or nano/microscale topographic features were performed using an identical procedure, with the exception that (i) all polymer solutions and rinse baths were replaced with new solutions or solvent after every individual dipping cycle, and (ii) lower molecular weight PVDMA synthesized in the absence of added oligomers (see above) was used. Flexible PET substrates and porous stainless steel mesh substrates were coated using procedures identical to those used for planar glass substrates. Microscale glass beads were coated using a similar protocol, with the following changes: (i) glass beads (1 g) were placed in a glass tube, the bottom of which was capped by fixing laboratory cleaning paper (Kimwipes; Kimberly-Clark Corp., Neenah, WI) across the opening using copper wire, and (ii) the glass tube containing the beads was then immersed into the dipping solutions and rinse baths. Coatings were characterized or used in subsequent experiments immediately or dried under a stream of filtered, compressed air and stored in a vacuum desiccator until use.

Functionalization and Chemical Patterning of Multilayer-Coated Substrates: Substrates coated with PEI/PVDMA multilayers were covalently functionalized by reaction with a variety of different hydrophilic amines (D-glucamine, DMAPA) and hydrophobic amines (*n*-propylamine, *n*-octylamine, and *n*-decylamine). Solutions of *n*-propylamine, *n*-octylamine, *n*-decylamine, and DMAPA (20×10^{-3} M) were prepared in THF, and solutions of D-glucamine were prepared using either DMSO or water. For experiments requiring functionalization over large areas, film-coated substrates were immersed completely in these solutions at room temperature for 2 h. Films were then rinsed liberally with THF or DMSO and acetone and dried with filtered air. To install anionic carboxylate groups, reactive coatings were immersed in alkaline phosphate buffer (pH = 9.75) to hydrolyze remaining azlactone functionality. For experiments in which patterns of both oil adhesive and non-oil-adhesive regions were desired (see text), reactive multilayers were first patterned with small hydrophilic spots by placing droplets of aqueous solutions of glucamine (20 μL of a 20 mg mL^{-1} glucamine solution in PBS buffer, pH = 9.0) for 10 min. These chemically patterned samples were then immersed in *n*-decylamine, using the procedure described above, to react with residual azlactone functionality and render the remainder of the surrounding regions of the films hydrophobic (and oil adhesive). Functionalized films were used in subsequent experiments immediately or were dried under a stream of filtered air and stored in a vacuum desiccator until use.

Characterization of Physical and Chemical Stability: A variety of physical and mechanical challenges and environmentally or chemically harsh conditions were used to characterize the stabilities of the underwater superoleophobic coatings. All of these tests were performed using coatings 10 bilayers thick and functionalized with D-glucamine. General protocols for each experiment are described below.

Sand Abrasion Tests: Sand abrasion tests were performed using dry films under air. Sand (10 g, grain size ranging from ≈90 to ≈400 μm) was poured slowly onto the coatings from a distance of 20 cm, and then the underwater oil advancing and receding contact angles were measured (see Figure S4, Supporting Information, for a schematic of the setup). SEM was used to characterize nanoscale and microscale surface morphologies before and after contact with the sand.

Adhesive Tape Peeling Tests: Adhesive tape peeling tests were performed by placing a strip of adhesive tape on the coatings using a pressure of ≈445 kPa, and then manually peeling the tape from the surfaces of the films. Underwater oil advancing and receding contact angles were then recorded. SEM was used to characterize nanoscale and microscale surface morphologies before and after placing and peeling the tape.

Sandpaper Abrasion Tests: Sandpaper abrasion tests were performed by repeated manual rubbing with abrasive sandpaper (2 μm grit) 25 times.

Underwater Abrasion and Impact Tests: Experiments to characterize the ability of hydrated films to withstand abrasion and impact were performed by placing films under 15 cm of water and then slowly pouring 50 g of solid glass beads (diameter = 2–3 mm) from a distance of 15 cm using a funnel fitted with a glass tube to direct the falling beads to the coatings (a schematic of this experimental setup is shown in Figure S4, Supporting Information). Underwater oil advancing and receding contact angles were then recorded. SEM was used to characterize nanoscale and microscale surface morphologies before and after contact with the glass beads.

Contact with Rapidly Flowing Water: Coatings were exposed to water ejected from a rapidly flowing faucet for 30 min. The flow rate of the faucet was 100 mL s^{-1} and the nozzle diameter was 1.0 cm, yielding a nozzle velocity of 127.4 cm s^{-1}. The substrate was held at a distance of ≈2 cm from the faucet. As the diameter of the water stream did not vary over this distance, we estimate the velocity of the stream just prior to contact to be ≈127 cm s^{-1}. Underwater oil advancing and receding contact angles were then recorded.

Bending and Creasing: Coatings fabricated on flexible sheets of PET were bent and flexed manually 50 times and then finally permanently creased by the application of moderate pressure. Measurements of contact angles made on creased films were performed by unfolding the substrate back into a flat sheet and placing droplets of oil in direct contact with the crease.

Exposure to Boiling Water: For experiments designed to characterize the impact of exposure to boiling water, coated glass slides were held in boiling water for 1 h. Underwater oil advancing and receding contact angles were then recorded.

Exposure to Freezing Conditions and Multiple Freeze/Thaw Cycles: For experiments designed to characterize the impact of the freezing of water within and around the coatings in aqueous environments, coated glass slides were immersed completely in deionized water and the whole system was placed in a freezer at a temperature of –25 °C for 6 h until all water was frozen solid. The resulting block of ice was removed from the freezer and allowed to thaw at room temperature. Underwater oil advancing and receding contact angles were then recorded. This cycle of freezing, thawing, and characterization was performed 10 times.

Exposure to Autoclaving Cycles: Coated glass slides were autoclaved for 40 min at 121 °C using an Allen-Bradley Panel View Plus 600 System. Underwater oil advancing and receding contact angles were then recorded.

Exposure to Extremes of pH: Coated glass slides were immersed in acidic (0.5 M HCl, pH = 1) and alkaline (0.5 M NaOH, pH = 11) solutions at ambient temperature for 30 min and then rinsed with deionized water. Underwater oil advancing and receding contact angles were then recorded.

Exposure to Extremes of Ionic Strength: Coated glass slides were immersed in simulated seawater and solutions of 1.0 M NaCl for 4 months at ambient temperature. Underwater oil advancing and receding contact angles were recorded periodically during these experiments.

Exposure to Aqueous Solutions Containing Surface-Active Agents: Coated glass slides were immersed in solutions containing high concentrations of cationic, anionic, and nonionic surfactants [sodium dodecyl sulfate (SDS, 5.0 M), dodecyltrimethylammonium bromide (DTAB, 5.0 M), and Triton X-100 (1.0 M)] and mammalian cell culture medium supplemented with 10% fetal bovine serum at ambient temperature for at least one month. Underwater oil advancing and receding contact angles were recorded periodically during these experiments.

Exposure to Eutrophic Lake Water: Coated glass slides were immersed in eutrophic lake water (Lake Mendota, Madison, Wisconsin) containing well-characterized concentrations of dissolved and suspended organic matter, inorganic compounds, and microbial flora at ambient temperature for at least 4 months. Underwater oil advancing and receding contact angles were recorded periodically during these experiments.

Characterization of Oil Droplets on Surfaces Patterned with Patches of Non-Adhesive and Adhesive Underwater Superoleophobicity: For these experiments (see Figure 4a,b), a circular spot with a diameter of ≈3 mm was selectively patterned on the surface of a glass slide coated with a reactive, azlactone-functionalized film by (i) treatment with a droplet of aqueous glucamine, and then (ii) the remainder of the surface of the film was functionalized by treatment with propylamine using methods described above. This procedure resulted in functional surfaces containing patterned spots that exhibited a circular region of non-adhesive underwater superoleophobicity surrounded by a background that exhibited adhesive underwater superoleophobicity. The patterned film was then placed horizontally under water and a 10 μL droplet of DCE (stained with Nile red) was placed on the circular (non-adhesive superoleophobic) region. Two additional reference droplets were placed on the surrounding (adhesive superoleophobic) region. One end of the glass substrate was then raised and fixed at a desired angle of incline (e.g., 4°), and the behaviors of the droplets were characterized and recorded using a digital camera (see Figure 4a,b and text for additional details).

Characterization of the Interaction of Oil/Water Emulsion Droplets with Film-Coated Beads: Experiments to characterize the nature of interactions between DCE and individual microscale beads coated with underwater superoleophobic films were conducted in the following general manner. An oil/water emulsion (20 mL, 1:10 v/v) was prepared by sonicating a mixture of water and DCE containing the water-insoluble red dye Nile red for 30 min at room temperature. Glass beads (200 mg; diameter = 200–300 μm) coated with films functionalized with either glucamine (to create coatings that exhibit non-adhesive superoleophobicity on planar glass) or decylamine (to create coatings that exhibit adhesive superoleophobicity on planar glass) using methods described above. Samples of each type of coated bead were then added to 1 mL of the oil/water emulsion, shaken continuously for 10 min, and then kept steady for another 20 min to promote physical interactions with oil droplets and allow the beads to settle. The glass beads were then separated from the supernatant, washed briefly with water, and the amount of Nile red-stained DCE on the surfaces of the beads was characterized by fluorescence microscopy.

Oil/Water Separation Using Stainless Steel Mesh Coated with Underwater Superoleophobic Films: Proof of concept demonstrations of the utility of these underwater superoleophobic coatings in the context of gravity-driven oil/water separation were performed in the following general manner. Samples of stainless steel wire mesh (1.5 × 2.5 cm, wire diameter ≈90 μm, pore size = 126.3 ± 3.5 μm) were coated using the protocol described above and then functionalized by treatment with D-glucamine. The coated mesh was then fixed between two halves of a disposable plastic funnel using epoxy and wet with water. A 12 mL mixture of conventional automotive motor oil and water (1:5, v/v) was then poured into the funnel. The water passed rapidly (in under one minute) through the coated mesh and into a collection vessel, and oil remained suspended on the coated mesh and was collected in near quantitative yield (see text). Subsequent experiments were performed and similar results were obtained using mixtures of automotive motor oil and water prepared using more complex aqueous phases, including alkaline (0.5 M, pH = 11) and acidic water (0.5 M, pH = 1), simulated seawater, and lake water.

Supporting Information

Supporting Information is available from the Wiley Online Library or from the author.

Acknowledgements

Financial support was provided by the NSF through a grant to the Materials Research Science and Engineering Center at UW-Madison (DMR-1121288) and the Office of Naval Research (N00014–07–1–0255 and N00014-14-1-0791). This work made use of NSF-supported shared facilities.

Received: October 24, 2014
Revised: January 7, 2015
Published online: February 4, 2015

[1] J. Genzer, K. Efimenko, *Science* **2000**, *290*, 2130.
[2] K. S. Liu, X. Yao, L. Jiang, *Chem. Soc. Rev.* **2010**, *39*, 3240.

[3] A. Tuteja, W. Choi, M. L. Ma, J. M. Mabry, S. A. Mazzella, G. C. Rutledge, G. H. McKinley, R. E. Cohen, *Science* **2007**, *318*, 1618.
[4] H. Bellanger, T. Darmanin, E. T. de Givenchy, F. Guittard, *Chem. Rev.* **2014**, *114*, 2694.
[5] X. Deng, L. Mammen, H. J. Butt, D. Vollmer, *Science* **2012**, *335*, 67.
[6] Z. L. Chu, S. Seeger, *Chem. Soc. Rev.* **2014**, *43*, 2784.
[7] J. K. Yuan, X. G. Liu, O. Akbulut, J. Q. Hu, S. L. Suib, J. Kong, F. Stellacci, *Nat. Nanotechnol.* **2008**, *3*, 332.
[8] B. Deng, R. Cai, Y. Yu, H. Q. Jiang, C. L. Wang, J. A. Li, L. F. Li, M. Yu, J. Y. Li, L. D. Xie, Q. Huang, C. H. Fan, *Adv. Mater.* **2010**, *22*, 5473.
[9] X. Yao, Y. L. Song, L. Jiang, *Adv. Mater.* **2011**, *23*, 719.
[10] M. H. Jin, J. Wang, X. Yao, M. Y. Liao, Y. Zhao, L. Jiang, *Adv. Mater.* **2011**, *23*, 2861.
[11] I. Banerjee, R. C. Pangule, R. S. Kane, *Adv. Mater.* **2011**, *23*, 690.
[12] A. K. Kota, G. Kwon, W. Choi, J. M. Mabry, A. Tuteja, *Nat. Commun.* **2012**, *3*, 1.
[13] E. Ueda, P. A. Levkin, *Adv. Mater.* **2013**, *25*, 1234.
[14] J. V. Timonen, M. Latikka, L. Leibler, R. H. Ras, O. Ikkala, *Science* **2013**, *341*, 253.
[15] Y. Tian, B. Su, L. Jiang, *Adv. Mater.* **2014**, *26*, 6872.
[16] W. Barthlott, C. Neinhuis, *Planta* **1997**, *202*, 1.
[17] X. F. Gao, L. Jiang, *Nature* **2004**, *432*, 36.
[18] W. G. Bae, H. N. Kim, D. Kim, S. H. Park, H. E. Jeong, K. Y. Suh, *Adv. Mater.* **2014**, *26*, 675.
[19] Y. Li, L. Li, J. Q. Sun, *Angew. Chem. Int. Ed.* **2010**, *49*, 6129.
[20] X. Deng, L. Mammen, Y. F. Zhao, P. Lellig, K. Mullen, C. Li, H. J. Butt, D. Vollmer, *Adv. Mater.* **2011**, *23*, 2962.
[21] U. Manna, D. M. Lynn, *Adv. Mater.* **2013**, *25*, 5104.
[22] T. Verho, C. Bower, P. Andrew, S. Franssila, O. Ikkala, R. H. Ras, *Adv. Mater.* **2011**, *23*, 673.
[23] L. Ionov, A. Synytska, *Phys. Chem. Chem. Phys.* **2012**, *14*, 10497.
[24] A. R. Parker, C. R. Lawrence, *Nature* **2001**, *414*, 33.
[25] M. J. Liu, S. T. Wang, Z. X. Wei, Y. L. Song, L. Jiang, *Adv. Mater.* **2009**, *21*, 665.
[26] Y. C. Jung, B. Bhushan, *Langmuir* **2009**, *25*, 14165.
[27] X. Liu, J. Zhou, Z. Xue, J. Gao, J. Meng, S. Wang, L. Jiang, *Adv. Mater.* **2012**, *24*, 3401.
[28] S. Nishimoto, B. Bhushan, *RSC Adv.* **2013**, *3*, 671.
[29] Y. Cai, L. Lin, Z. X. Xue, M. J. Liu, S. T. Wang, L. Jiang, *Adv. Funct. Mater.* **2014**, *24*, 809.
[30] L. Lin, M. J. Liu, L. Chen, P. P. Chen, J. Ma, D. Han, L. Jiang, *Adv. Mater.* **2010**, *22*, 4826.
[31] L. P. Xu, J. Zhao, B. Su, X. L. Liu, J. T. Peng, Y. B. A. Liu, H. L. Liu, G. Yang, L. Jiang, Y. Q. Wen, X. J. Zhang, S. T. Wang, *Adv. Mater.* **2013**, *25*, 606.
[32] L. P. Xu, J. T. Peng, Y. B. Liu, Y. Q. Wen, X. J. Zhang, L. Jiang, S. T. Wang, *ACS Nano* **2013**, *7*, 5077.
[33] W. Ma, H. Xu, A. Takahara, *Adv. Mater. Interfaces* **2014**, *1*, 1300092.
[34] X. L. Liu, J. Gao, Z. X. Xue, L. Chen, L. Lin, L. Jiang, S. T. Wang, *ACS Nano* **2012**, *6*, 5614.
[35] W. B. Zhang, Z. Shi, F. Zhang, X. Liu, J. Jin, L. Jiang, *Adv. Mater.* **2013**, *25*, 2071.
[36] M. E. Buck, J. Zhang, D. M. Lynn, *Adv. Mater.* **2007**, *19*, 3951.
[37] M. E. Buck, A. S. Breitbach, S. K. Belgrade, H. E. Blackwell, D. M. Lynn, *Biomacromolecules* **2009**, *10*, 1564.
[38] M. E. Buck, D. M. Lynn, *ACS Appl. Mater. Interfaces* **2010**, *2*, 1421.
[39] A. H. Broderick, U. Manna, D. M. Lynn, *Chem. Mater.* **2012**, *24*, 1786.
[40] U. Manna, A. H. Broderick, D. M. Lynn, *Adv. Mater.* **2012**, *24*, 4291.
[41] P. A. Levkin, F. Svec, J. M. J. Frechet, *Adv. Funct. Mater.* **2009**, *19*, 1993.
[42] G. C. Bortleson, G. F. Lee, *Environ. Sci. Technol.* **1972**, *6*, 799.
[43] T. D. Brock, J. Clyne, *Appl. Environ. Microbiol.* **1984**, *47*, 731.
[44] A. B. D. Cassie, S. Baxter, *Trans. Faraday Soc.* **1944**, *40*, 546.
[45] R. N. Wenzel, *Ind. Eng. Chem.* **1936**, *28*, 988.
[46] R. G. Chapman, E. Ostuni, S. Takayama, R. E. Holmlin, L. Yan, G. M. Whitesides, *J. Am. Chem. Soc.* **2000**, *122*, 8303.
[47] B. P. Orner, R. Derda, R. L. Lewis, J. A. Thomson, L. L. Kiessling, *J. Am. Chem. Soc.* **2004**, *126*, 10808.
[48] Y. Huang, M. J. Liu, J. X. Wang, J. M. Zhou, L. B. Wang, Y. L. Song, L. Jiang, *Adv. Funct. Mater.* **2011**, *21*, 4436.
[49] A. H. Broderick, M. R. Lockett, M. E. Buck, Y. Yuan, L. M. Smith, D. M. Lynn, *Chem. Mater.* **2012**, *24*, 938.
[50] M. E. Buck, S. C. Schwartz, D. M. Lynn, *Chem. Mater.* **2010**, *22*, 6319.